arXiv:hep-ph/9806265v1 4 Jun 1998

ANL-HEP-PR-98-39

JLAB-THY-98-22

June 2, 1998

# Spin Dependence of Associated Production of a Prompt Photon and a Charm Quark at Next-to-Leading Order in QCD

Edmond L. Berger[a] and Lionel E. Gordon[b,c]

[a] *High Energy Physics Division, Argonne National Laboratory, Argonne, IL 60439*

[b] *Jefferson Lab, Newport News, VA 23606*

[c] *Hampton University, Hampton, VA 23668*

## Abstract

A second order, $O(\alpha_s^2)$, calculation in perturbative quantum chromodynamics is presented of the longitudinal spin dependence of the cross section for the two particle inclusive reaction $p + p \to \gamma + c + X$ for large values of the transverse momentum of the prompt photon and charm quark. Differential distributions are provided for the spin-averaged cross section and for the two-spin longitudinal polarization asymmetry $A_{LL}$ at the energy of the Brookhaven Relativistic Heavy Ion Collider. An assessment is given of the prospects for determination of the spin dependence of the charm quark density.

Typeset using REVTEX

## I. INTRODUCTION

Because they couple in a point-like fashion to quarks, the observation of photons with large values of transverse momentum in a high energy hadron collision has long been regarded as an incisive probe of short distance dynamics. The dominance of the Compton subprocess $q + g \to \gamma + q$ at both leading- and at next-to-leading orders [1] in perturbative quantum chromodynamics [QCD] makes spin-averaged inclusive prompt photon production the reaction of choice for investigations of the magnitude and Bjorken $x$ dependence of the gluon density of the incident hadrons, $G(x, \mu)$. The Compton subprocess also dominates the dynamics in longitudinally polarized proton-proton reactions [2,3] as long as the polarized gluon density $\Delta G(x, \mu)$ is not too small. As a result, two-spin measurements of inclusive prompt photon production in polarized $pp$ scattering should constrain the size, *sign*, and Bjorken $x$ dependence of $\Delta G(x, \mu)$.

In previous papers we investigated the associated production of a prompt photon along with a charm quark [4,5], $p + \bar{p} \to \gamma + c + X$, in spin-averaged reactions at high energy. We showed that collider data from this two-particle inclusive reaction at large values of transverse momentum may be used to measure the spin-averaged charm quark density in the nucleon. In this paper, we extend our previous work by including a full next-to-leading order treatment of the longitudinal spin dependence. We specialize to $p + p \to \gamma + c + X$ at the energies of the Brookhaven Relativistic Heavy Ion Collider (RHIC) facility.

For values of the transverse momentum $p_T^c$ of the charm quark much larger than the mass $m_c$ of the quark, only one *direct* hard scattering subprocess contributes in leading order: the quark-gluon Compton subprocess $gc \to \gamma c$. The initial charm quark and the initial gluon are constituents of the initial hadrons. In addition, there is a leading order *fragmentation* process in which the photon is produced from quark or gluon fragmentation, e.g., $gg \to c\bar{c}$ followed by $\bar{c} \to \gamma X$, or $qc \to qc$ followed by $q \to \gamma$. At next-to-leading order in QCD, several subprocesses contribute to the $\gamma + c + X$ final state: $gc \to gc\gamma$, $gg \to c\bar{c}\gamma$, $q\bar{q} \to c\bar{c}\gamma$, $qc \to qc\gamma$, $\bar{q}c \to \bar{q}c\gamma$, $c\bar{c} \to c\bar{c}\gamma$, and $cc \to cc\gamma$. A full next-to-leading

order calculation requires the computation of the hard-scattering matrix elements for these two-to-three particle production processes as well as the one-loop $O(\alpha_s^2)$ corrections to the lowest order subprocess $gc \to \gamma c$.

We are interested ultimately in the fully differential two-particle inclusive cross section, $E_\gamma E_c d\sigma/d^3p_\gamma d^3p_c$, where $(E, p)$ represents the four-vector momentum of the $\gamma$ or $c$ quark. For each contributing subprocess, this calculation requires integration over the momentum of the unobserved final parton in the two-to-three particle subprocesses ($g$, $\bar{c}, q$, or $\bar{q}$). Collinear singularities must be handled analytically by dimensional regularization and absorbed into parton momentum densities or fragmentation functions. In the theoretical analysis reported here, a combination of analytic and Monte Carlo integration methods is used to perform phase-space integrations over unobserved final-state partons and the momenta of the initial partons. This approach facilitates imposition of photon isolation restrictions and other selections of relevance in experiments. We work in the massless approximation, $m_c = 0$. To warrant use of perturbation theory and the massless approximation, we limit our considerations to values of transverse momenta of the photon and charm quark $p_T^{\gamma,c} > 5$ GeV.

In the lowest order direct subprocess, $gc \to \gamma c$, the prompt photon emerges in isolation from the only other particle in the hard scattering, the charm quark. Long-distance quark-to-photon and gluon-to-photon fragmentation processes have been emphasized theoretically [6] and parametrized phenomenologically in leading order [7], and evolved in next-to-leading order [8,9]. These terms may account for more than half of the calculated inclusive single photon cross section at modest values of transverse momentum at collider energies. Photons originating through fragmentation are likely to emerge in the neighborhood of associated hadrons. An experimental isolation restriction is needed before a clean identification can be made of the photon and a measurement made of its momentum. Isolation reduces the size of the observed fragmentation contribution. Photon isolation complicates the theoretical interpretation of results, however, since it threatens to upset the cancellation of infra-red divergences in perturbation theory [10]. In this paper, we include the fragmentation contributions, and we impose isolation requirements through our Monte Carlo method.

A combination of analytic and Monte Carlo methods similar to that we employ in this paper has been used to carry out next-to-leading order QCD calculations of other processes including unpolarized and polarized inclusive prompt photon [11,12], unpolarized and polarized prompt photon plus jet production [13,14] and unpolarized and polarized photon pair [15,16] production in hadron collisions, single [17] and pair production of heavy gauge bosons [18], and in our earlier work on spin-averaged $\gamma c$ production [5]. The combination of analytic and Monte Carlo techniques used here to perform the phase space integrals is documented and described in detail elsewhere [11,15,17,18,5,16] with some details specific to the polarized case discussed in Ref. [16]. We refer readers to those papers for further details.

After theoretical expressions are derived in perturbative QCD that relate the spin-dependent cross section at the hadron level to spin-dependent partonic hard-scattering matrix elements and polarized parton densities, we must adopt models for spin-dependent parton densities in order to obtain illustrative numerical expectations. For the spin-dependent gluon density that we need, we use the three different parametrizations of $\Delta G(x,\mu)$ suggested in Ref. [19]. We generate the spin dependent polarized charm quark densities $\Delta c(x,\mu)$ perturbatively from these polarized gluon densities, beginning with the assumption that $\Delta c(x,\mu_o) = 0$ at the starting value for evolution $\mu_o = 1.5$ GeV. Our polarized gluon and charm quark densities satisfy expected positivity constraints.

We present spin-averaged cross sections differential in the transverse momenta and rapidities of the photon and charm quark in $pp$ collisions at the center-of-mass energy $\sqrt{S} = 200$ GeV typical of the Brookhaven RHIC collider. Our results on the longitudinal spin dependence are expressed in terms of the two-spin longitudinal asymmetry $A_{LL}$, defined by

$$A_{LL} = \frac{\sigma^{\gamma,c}(+,+) - \sigma^{\gamma,c}(+,-)}{\sigma^{\gamma,c}(+,+) + \sigma^{\gamma,c}(+,-)}, \tag{1.1}$$

where $+,-$ denote the helicities of the incoming protons.

In Section II, we describe the next-to-leading order calculation of the spin-dependent cross section in perturbative QCD. Parametrizations of the spin-dependent gluon and charm

quark densities are discussed in Sec. III. Differential cross sections and other numerical results are presented in Section IV. Summary remarks are collected in Section V. An appendix is included in which we derive analytic expressions for some of the parton level spin-dependent cross sections.

## II. CONTRIBUTIONS THROUGH NEXT-TO-LEADING ORDER

The two-particle inclusive hadron reaction $h_1+h_2 \to \gamma+c+X$ proceeds through partonic hard-scattering processes involving initial-state light quarks $q$ and gluons $g$. In lowest-order QCD, at $\mathcal{O}(\alpha_s)$, the only *direct* partonic subprocess is $c+g \to \gamma+c$. In addition, there is a leading order *fragmentation* process in which the photon is produced from quark or gluon fragmentation, e.g., $gg \to c\bar{c}$ followed by $\bar{c} \to \gamma X$, or $qc \to qc$ followed by $q \to \gamma$. Calculations of the cross section at order $\mathcal{O}(\alpha_s^2)$ involve virtual gluon loop corrections to the $\mathcal{O}(\alpha_s)$ direct subprocess as well as real gluon radiation contributions from a wide range of $2 \to 3$ parton subprocesses (of which some examples are shown in Fig. 1(c).)

The full set of three-body final-state subprocesses is:

$$g + c \to g + c + \gamma \tag{2.1a}$$

$$g + g \to c + \bar{c} + \gamma \tag{2.1b}$$

$$q + \bar{q} \to c + \bar{c} + \gamma \tag{2.1c}$$

$$q + c \to q + c + \gamma \tag{2.1d}$$

$$\bar{q} + c \to \bar{q} + c + \gamma \tag{2.1e}$$

$$c + \bar{c} \to c + \bar{c} + \gamma \tag{2.1f}$$

$$c + c \to c + c + \gamma \tag{2.1g}$$

The physical cross section is obtained through the factorization theorem,

$$\frac{d^2\sigma^{\gamma,c}_{h_1h_2}}{dp_T^c dp_T^\gamma dy_c dy_\gamma d\phi} \sim \sum_{ij} \int dx_1 dx_2 f^i_{h_1}(x_1,\mu_f) f^j_{h_2}(x_2,\mu_f) \frac{s d^2\hat{\sigma}^{\gamma,c}_{ij}}{dt du}(s, p_T, y, \phi; \mu_f). \tag{2.2}$$

It depends on the hadronic center-of-mass energy $S$, the transverse momenta $p_T^c$ and $p_T^\gamma$ of the charm quark and photon, the rapidities $y_c$ and $y_\gamma$, and the relative azimuthal angle $\phi$; $\mu_f$ is the factorization scale of the scattering process. The usual Mandelstam invariants in the partonic system are defined by $s = (p_1 + p_2)^2$, $t = (p_1 - p_\gamma)^2$, and $u = (p_2 - p_\gamma)^2$, where $p_1$ and $p_2$ are the momenta of the initial state partons and $p_\gamma$ is the momentum of the final photon. The indices $ij$ label the initial parton channels whose contributions are added incoherently to yield the total physical cross section. The spin-averaged parton densities are denoted $f_h(x, \mu_f)$. The partonic hard-scattering cross section $\hat{\sigma}_{ij}^{\gamma,c}(s, p_T, y, \phi; \mu_f)$ is obtained commonly from fixed-order QCD calculations through

$$\frac{d^2\hat{\sigma}_{ij}^{\gamma,c}}{dtdu} = \alpha_s(\mu^2)\frac{d^2\hat{\sigma}_{ij}^{\gamma,c,(a)}}{dtdu} + \alpha_s^2(\mu^2)\frac{d^2\hat{\sigma}_{ij}^{\gamma,c,(b)}}{dtdu} + \alpha_s^2(\mu^2)\frac{d^2\hat{\sigma}_{ij}^{\gamma,c,(c)}}{dtdu} + \mathcal{O}(\alpha_s^3). \tag{2.3}$$

The tree, virtual loop, and real emission contributions are labeled (a), (b), and (c). The parameter $\mu$ is the renormalization scale.

The longitudinal spin-dependent cross section for $h_1 + h_2 \to \gamma + c + X$ is very similar to Eq. (2.2):

$$\frac{d^2\Delta\sigma_{h_1h_2}^{\gamma,c}}{dp_T^c dp_T^\gamma dy_c dy_\gamma d\phi} \sim \sum_{ij}\int dx_1 dx_2 \Delta f_{h_1}^i(x_1, \mu_f)\Delta f_{h_2}^j(x_2, \mu_f)\frac{s d^2\Delta\hat{\sigma}_{ij}^{\gamma,c}}{dtdu}(s, p_T, y, \phi; \mu_f). \tag{2.4}$$

The polarized parton densities are defined by

$$\Delta f_h^i(x, \mu_f) = f_{h,+}^i(x, \mu_f) - f_{h,-}^i(x, \mu_f), \tag{2.5}$$

where $f_{h\pm}^i(x, \mu_f)$ is the distribution of parton of type $i$ with positive $(+)$ or negative $(-)$ helicity in hadron $h$. Likewise, the polarized partonic cross section $\Delta\hat{\sigma}^{\gamma,c}$ is defined by

$$\Delta\hat{\sigma}^{\gamma,c} = \hat{\sigma}^{\gamma,c}(+,+) - \hat{\sigma}^{\gamma,c}(+,-), \tag{2.6}$$

with $+, -$ denoting the helicities of the incoming partons.

### A. Leading order contributions

In leading order in perturbative QCD, only one *direct* subprocess contributes to the hard-scattering cross section, the QCD Compton process $cg \to \gamma c$, unlike the case for

single inclusive prompt photon production, where the annihilation process $q\bar{q} \to \gamma g$ also contributes. Since the leading order direct partonic subprocess has a two-body final state, the photon and $c$ quark are produced with balancing transverse momenta. In addition, there are effectively leading-order contributions in which the photon is produced by fragmentation from a final-state parton. These are

$$\begin{aligned} c + g &\to g + c \\ g + g &\to c + \bar{c} \\ c + q &\to c + q \\ c + \bar{q} &\to c + \bar{q} \\ c + c &\to c + c \\ c + \bar{c} &\to c + \bar{c} \\ q + \bar{q} &\to c + \bar{c}. \end{aligned} \tag{2.7}$$

If the photon is to be isolated from the observed charm quark, it arises from fragmentation of the gluon $g$ and the non-charm quark $q$, respectively, in the cases of the first, third and fourth processes. In the other cases it is produced by fragmentation of one of the (anti)charm quarks.

In a fully consistent next-to-leading order calculation, one should calculate the subprocesses in Eq. (2.7) to $O(\alpha_s^3)$, since the photon fragmentation functions that are convoluted with the hard subprocess cross sections are of $O(\alpha_{em}/\alpha_s)$. For simplicity, we include them in $O(\alpha_s^2)$ only. In fact, next-to-leading order fragmentation contributions to single prompt photon production have been included only once before [20,12]. We expect the next-to-leading order corrections to the fragmentation contributions to be insignificant numerically especially after isolation cuts are imposed. This expectation is confirmed by a study performed in Ref. [21] on inclusive prompt photon production in the polarized case. It was also shown in Ref. [21] that predictions for the asymmetries are hardly affected by inclusion of the fragmentation contributions either before or after isolation of the photon.

### B. Next-to-leading order contributions

There are two classes of contributions in next-to-leading order. There are the virtual gluon exchange corrections to the lowest order process, $cg \to \gamma c$. Examples are shown in Fig.1(b). These amplitudes interfere with the Born amplitudes and contribute at $O(\alpha_{em}\alpha_s^2)$. They were calculated twice before in the spin-averaged case [22,23]. At next-to-leading order there are also three-body final-state contributions, listed in Eq. (2.1). Both the spin dependent and spin-averaged virtual loop and three-body matrix elements are taken from Ref. [23], where they are calculated for single inclusive prompt photon production.

In Ref. [23] the original 'tHooft-Veltman-Breitenlohner-Maison (TVBM) [24,25] scheme was used to treat the 4-dimensional $\gamma_5$ matrix and antisymmetric $\epsilon_{\mu\nu\rho\sigma}$ tensor in $n$ dimensions. These objects arise when the traces are taken to calculate the helicity dependent matrix elements. To project onto definite helicity states, $h$, for (anti-) quarks and $\lambda$ for gluons, the relations

$$u(p,h)\bar{u}(p,h) = \frac{1}{2}\gamma^{\mu}(p)(1 - h\gamma_5) \tag{2.8}$$

and

$$\epsilon_{\mu}(p,\lambda)\epsilon^{*}_{\nu}(p,\lambda) = \frac{1}{2}\left[-g_{\mu\nu} + i\lambda\epsilon_{\mu\nu\rho\sigma}\frac{p^{\rho}p'^{\sigma}}{p.p'}\right] \tag{2.9}$$

are used. In the TVBM scheme, $n$-dimensional Minkowski space is divided into a 4-dimensional and a $(n-4)$-dimensional part. Any vector $k$ has a 4-dimensional, $\hat{\hat{k}}$, and a $(n-4)$-dimensional part, $\hat{k}$. This means that the $n$ dimensional matrix elements calculated in Ref. [23] contain products of these $(n-4)$-dimensional 'hat' momenta. In Ref. [23] it was shown that these contributions are non-zero in the collinear limit only, and thus in our case they are included in the hard collinear integrals given in the appendix. A detailed account of all aspects of the phase space integration will be given elsewhere [26]. It should be mentioned here that the matrix elements were also calculated in Ref. [27] in a scheme different from the TVBM scheme outlined here. Their results seem similar to those of Ref. [23], but a detailed comparison of the matrix elements has not yet been made.

The main task of our calculation is to integrate the three-body matrix elements over the phase space of the unobserved particle in the final state. The situation here is different from the standard case of single inclusive particle production because we wish to retain as much control as possible over the kinematic variables of a second particle in the final state, while at the same time integrating over enough of the phase space to ensure cancellation of all infrared and collinear divergences, inherent when massless particles are assumed. All the processes of Eq. (2.1), except the first, involve collinear singularities but no soft singularities. The soft and collinear singularities are first exposed by integrating the three-body phase space in $n$-dimensions over the soft and collinear regions of phase space. These soft and collinear regions are separated from the rest of the three body phase space by introducing soft and collinear cut-off parameters $\delta_s$ and $\delta_c$. The collinear and soft singularities are cancelled and factored in the $\overline{MS}$ scheme as explained in Ref. [5].

At $O(\alpha_s^2)$ there are, in addition, fragmentation processes in which the hard-scattering two-particle final-state subprocesses

$$\begin{aligned} c + g &\to \gamma + c \\ c + \bar{c} &\to \gamma + g \\ q + \bar{q} &\to \gamma + g \end{aligned} \tag{2.10}$$

are followed by fragmentation processes $c \to cX$, in the case of the first subprocess, and $g \to cX$ in the cases of the last two. These should be included because we have factored the collinear singularities in the corresponding three-body final-state processes into non-perturbative fragmentation functions for production of a charm quark from a particular parton. As a first approximation, we estimate these fragmentation functions by

$$D_{c/c}(z, \mu^2) = \frac{\alpha_s(\mu^2)}{2\pi} P_{qq}(z), \tag{2.11}$$

and

$$D_{c/g}(z, \mu^2) = \frac{\alpha_s(\mu^2)}{2\pi} P_{qg}(z), \tag{2.12}$$

where $P_{ij}(z)$ are the lowest order splitting functions for parton $j$ into parton $i$ [28]; and $\alpha_s(\mu^2)$ is the strong coupling strength.

For completeness we have gathered some of the main ingredients used in calculating the polarized cross section in the appendix. Similar results for the unpolarized case can be found in Ref. [5]. Further details and a complete list of the 4-dimensional three-body final-state matrix elements will be given in Ref. [26].

## III. POLARIZED PARTON DENSITIES

Our spin-dependent gluon density and our spin-dependent up, down, and strange quark densities (and their antiquark components) are adapted from the set of polarized parton densities published by Gehrmann and Stirling (GS) [19]. However, this set of spin-dependent densities, as well as other recent parametrizations available for general use, does not include a charm contribution [30]. At the values of squared four-momentum transfer, $Q^2$, at which spin-dependent deep-inelastic scattering data have been obtained, the charm contribution is expected to be very small. Fits to the data are thus insensitive to the charm contribution. The situation is somewhat different in the spin-averaged case, and mechanisms for inclusion of charm are in general use.

In particular, a charm component is included in the CTEQ4M spin-averaged parametrization [31] at a scale $\mu_o = m_c$, where $m_c \sim 1.5$ GeV is the charm quark mass. At this threshold scale the charm quark density is assumed to have zero value, $c(x, \mu_o) = 0$. Non-zero charm quark and antiquark densities are generated at larger values of $\mu$ via the DGLAP perturbative QCD evolution equations through gluon splitting into $c\bar{c}$ pairs. Since we use the CTEQ4M distributions [31] as our spin-averaged parton densities, it is reasonable to use a similar mechanism to generate the spin-dependent charm densities, with spin-dependent Altarelli-Parisi splitting functions used in the evolution.

The evolution mechanism outlined above implies that the spin-dependent charm quark density will depend strongly on the assumed value of the spin-dependent gluon density.

Uncertainty in knowledge of the gluon density will propagate to the charm density. The current deep inelastic scattering data do not constrain the polarized gluon density very tightly, and most groups present more than one plausible parametrization. Gehrmann and Stirling [19] present three such parametrizations, labelled GSA, GSB, and GSC. In our parametrizations of the spin-dependent densities we begin with the GS parametrizations as our initial set at a scale $\mu_o = m_c$, and we evolve them to obtain spin-dependent gluon and quark densities at greater values of $\mu$, including a spin-dependent charm quark density. We use next-to-leading order DGLAP evolution equations with the number of flavors, $n_f = 4$. Details of the $x$-space evolution will be reported elsewhere Ref. [32]. Our approach is to adopt the GS polarized parton densities as our starting values and to extend them to include charm.

In Fig. 2(a), we display the ratio of our spin-dependent and spin-independent gluon densities, $\Delta G(x,\mu)/G(x,\mu)$, at the hard scale $\mu^2 = 100$ GeV$^2$ for the GSA, GSB, and GSC choices. In the GSA and GSB sets, $\Delta G(x,\mu_o)$ is positive for all $x$, whereas in the GSC set $\Delta G(x,\mu_o)$ changes sign. After evolution to $\mu^2 = 100$ GeV$^2$, $\Delta G(x,\mu)$ remains positive for essentially all $x$ in all three sets, but its magnitude is small in the GSB and GSC sets. In Fig. 2(b), we show the spin-dependent charm quark distributions. Positivity is well satisfied, as it is for $\Delta G(x,\mu)/G(x,\mu)$. The value of $\Delta c(x,\mu)/c(x,\mu)$ is reasonably substantial in the GSA case, reflecting the large size of $\Delta G(x,\mu)$ from which $\Delta c(x,\mu)$ is generated. The size of $\Delta c(x,\mu)/c(x,\mu)$ is correspondingly smaller in the GSB and GSC cases, hovering near zero in the GSC case.

As mentioned, our charm quark densities depend on the choice made for the gluon densities. In addition, we assume that there is no intrinsic charm quark density. If an intrinsic density were adopted, one might begin with non-zero charm and anti-charm densities at $\mu_o$ whose $x$-dependences need not be assumed identical, in both the spin-averaged and spin-dependent cases. In a sense, our assumed forms for the spin-dependent charm quark densities represent the most conservative possibilities, and one should be alert experimentally to more interesting outcomes.

## IV. NUMERICAL RESULTS

In this section we present and discuss spin-averaged differential cross sections and two-spin longitudinal asymmetries for the joint production of a charm quark and a photon at large values of transverse momentum. All results are displayed for $pp$ collisions at the center-of-mass energy $\sqrt{S} = 200$ GeV typical of the Brookhaven RHIC collider. To obtain the spin-averaged differential cross sections presented in this paper, we convolute our hard-scattering matrix elements with the CTEQ4M parton densities [31]. We use the standard two-loop formula for the strong coupling strength with four massless flavors of quarks. We set $\Lambda^{(5)}_{QCD} = 0.202$ GeV (the CTEQ4M value). The spin-dependent parton densities are described in Sec. III.

Very similar differential distributions may be obtained if other parton sets are used instead, with quantitative differences reflecting differences among gluon and charm quark densities in the different sets [4]. We set the renormalization, factorization, and fragmentation scales to a common value $\mu = p_T^\gamma$ in most of our calculations. Since there are two observed particles in the final state, the charm quark and the photon, both of whose transverse momenta are large, an alternative choice might be $\mu = p_T^c$ or some function of $p_T^\gamma$ and $p_T^c$. The results of our calculations show that the magnitudes of $p_T^\gamma$ and $p_T^c$ tend to be comparable and that dependence of the cross sections on $\mu$ is slight. Therefore, choices of $\mu$ different from $\mu = p_T^\gamma$ should not produce significantly different answers, and we have verified this supposition in representative cases.

In collider experiments a photon is observed and its momentum is well measured only when the photon is isolated from neighboring hadrons. In our calculation, we impose isolation in terms of the cone variable $R$:

$$\sqrt{(\Delta y)^2 + (\Delta\phi)^2} \leq R. \tag{4.1}$$

In Eq. (4.1), $\Delta y$ ($\Delta\phi$) is the difference between the rapidity (azimuthal angle in the transverse plane) of the photon and that of any parton in the final state. The photon is said to be

isolated in a cone of size $R$ if the ratio of the hadronic energy in the cone and the transverse momentum of the photon does not exceed $\epsilon = 2\text{GeV}/p_T^\gamma$. We show distributions for the choice $R = 0.7$.

In Fig. 3(a) we show the spin-averaged differential cross section as a function of the transverse momentum of the photon $p_T^\gamma$, having restricted the transverse momentum of the charm quark to the range $p_T^c \geq 5$ GeV. The rapidities of the charm quark and photon are restricted to the central region, $-1 \leq y^{\gamma,c} \leq 1$ in order to mimic the central region coverage of the major detectors at RHIC. The solid curve shows our prediction when contributions are included from all subprocesses through $O(\alpha_s^2)$. The dominance of the $cg$ subprocess is illustrated by our dashed curve. This dominance is the basis for the statement that the spin-averaged cross section at collider energies can be used to determine the magnitude and Bjorken $x$ dependence of the spin-averaged charm quark density [4,5].

In Figs. 3(b) and (c), we present the two-spin longitudinal asymmetries, $A_{LL}$, as a function of $p_T^\gamma$, for the same kinematic selections as made for Fig. 3(a). Results are shown for three choices of the polarized gluon density (and, correspondingly, for the polarized charm quark density). The asymmetry becomes sizeable for large enough $p_T^\gamma$ only in the case of the GSA parton set.

As noted above the $cg$ subprocess dominates the *spin-averged* cross section. It is interesting and important to inquire whether this dominance persists in the spin-dependent situation. The dot-dashed curve in Fig. 3(b) shows the contribution to the asymmetry from the polarized $cg$ subprocesses in the case of the GSA set. It is positive for all $p_T^\gamma$. At small $p_T^\gamma$, the net asymmetry is driven negative by a large contribution from the $gg$ subprocess. For this GSA set, we see that once it becomes sizable (e.g., 5% or more), the total asymmetry from all subprocesses is dominated by the large contribution from the $cg$ subprocess. In Fig. 3(c), using a more expanded scale, we replot the overall asymmetry for the GSC choice of the polarized gluon density, and we also show the contribution from the $cg$ subprocess alone. In this case, the overall asymmetry $A_{LL}$ itself is small, and the contribution from the $cg$ subprocess cannot be said to dominate the answer.

In interpreting the results presented in Figs. 3(b) and (c), we begin with the supposition that the polarized gluon density will have been determined from data on inclusive prompt photon production. The question to pose is whether asymmetries of the type shown in Figs. 3(b) and (c) could shed light on the polarization of the charm quark density. If a large asymmetry is measured, similar to that expected in the GSA case at the larger values of $p_T^\gamma$, Fig. 3(b) shows that the answer is dominated by the $cg$ contribution, and the data will serve to constrain $\Delta c(x,\mu)$. On the other hand, if $\Delta G(x,\mu)$ is small and a small asymmetry is measured, such as shown in Fig. 3(c), one will not be able to conclude which of the subprocesses is principally responsible, and no information could be adduced about $\Delta c(x,\mu)$.

In Fig. 4 we show distributions in the rapidity of the charm quark, $y^c$, for $-1 \le y^\gamma \le 1$, $p_T^c \ge 5$ GeV, and 4 GeV $\le p_T^\gamma \le 50$ GeV. The spin-averaged distribution in $y^c$, shown in Fig. 4(a) is fairly broad, with full-width at half-maximum of nearly 3 units in rapidity. The dashed curve in Fig. 4(a) shows that the contribution from the $cg$ subprocess is dominant. The asymmetries are shown in Fig. 4(b) as functions of $y^c$. They are small for all three choices of the the polarized gluon density. These results are consistent with those shown in Fig. 3(b), although they might not appear to be at first glance. One must bear in mind that it is the region of relatively small $p_T^\gamma$ that dominates the integral over $p_T^\gamma$. The asymmetries shown in Fig. 3(b) are small at modest values of $p_T^\gamma$. In the GSA case, the total asymmetry at relatively small values of $p_T^\gamma$ is opposite in sign to the positive contribution from the $cg$ subprocess.

The structure of the QCD hard-scattering matrix element produces *positive* correlations in rapidity [29] at collider energies. To examine correlations more precisely, we study the spin-averaged cross section and the asymmetry as functions of the difference of the rapidities of the photon and charm quark. Results are shown in Fig. 5.

## V. SUMMARY AND DISCUSSION

In this paper we present the results of a calculation of the longitudinal spin-dependence of the inclusive production of a prompt photon in association with a charm quark at large values of transverse momentum. This analysis is done at next-to-leading order in perturbative QCD. We employ a combination of analytic and Monte Carlo integration methods in which infrared and collinear singularities of the next-to-leading order matrix elements are handled properly. We provide differential cross sections and polarization asymmetries as functions of transverse momenta and rapidity, including photon isolation restrictions, that may be useful for estimating the feasibility of measurements of the spin-averaged and spin-dependent cross sections in future experiments at RHIC collider energies. We show that the study of two-particle inclusive spin-averaged distributions, with specification of the momentum variables of both the final prompt photon and the final heavy quark, tests correlations inherent in the QCD matrix elements [29] and should provide a means for measuring the charm quark density in the nucleon [4]. In the spin-dependent case, significant values of $A_{LL}$ (i.e., greater than 5 %) may be expected for $p_T^\gamma > 15$ GeV if the polarized gluon density $\Delta G(x,\mu)$ is as large as that in the GSA set of polarized parton densities. If so, the data on associated production could be used to determine the polarization of the charm quark density in the nucleon. On the other hand, for small $\Delta G(x,\mu)$, dominance of the $cg$ subprocess is lost, and $\Delta c(x,\mu)$ is inaccessible.

Our spin-averaged and polarized charm quark densities are generated perturbatively from gluon splitting into charm quark and charm antiquark pairs. They depend entirely on the choice made for the gluon densities: a small polarized gluon density leads to a small polarized charm density. Reality may well be different. For example, there could be a non-perturbative intrinsic charm quark component. In a sense, our assumed forms for the spin-averaged and spin-dependent charm quark densities represent the most conservative possibilities.

In a typical experiment, the momentum of the quark may be inferred from the momen-

tum of prompt lepton decay products or the momentum of charm mesons, such as $D^*$'s. Alternatively, our distributions in $p_T^c$ may be convoluted with charm quark fragmentation functions, deduced from, e.g., $e^+e^-$ annihilation data, to provide distributions for the prompt leptons or $D^*$'s.

## VI. ACKNOWLEDGMENTS

The work at Argonne National Laboratory was supported by the US Department of Energy, Division of High Energy Physics, Contract number W-31-109-ENG-38.

## APPENDIX A: ANALYTIC EXPRESSIONS

In order to make this paper reasonably self-contained, we collect in this appendix all the formulae we use in the calculation of the polarized cross section. We label the momenta for the generic three-body final-state process by

$$p_1 + p_2 \to p_3 + p_4 + p_5, \tag{A1}$$

where $p_3$ denotes the photon and $p_4$ denotes the observed charm quark, and we define the usual Mandelstam invariants

$$\begin{aligned} \hat{t} &= (p_1 - p_3)^2 \\ \hat{u} &= (p_2 - p_3)^2 \\ \hat{s} &= (p_1 + p_2)^2. \end{aligned} \tag{A2}$$

We express the two-body final-state cross sections in terms of the scaled variable $v$, where

$$v = 1 + \frac{\hat{t}}{\hat{s}}. \tag{A3}$$

### 1. Two-body contributions

The effective two-body contribution includes the $O(\alpha_s^2)$ virtual gluon-exchange loop contributions and the soft and/or collinear parts of the three-body contributions (this remark applies to initial-state collinear contributions only, as explained later). After all soft pole singularities are cancelled and all collinear pole singularities are factored, the effective two-body contribution is expressed as

$$\begin{aligned} \Delta\sigma_{2body}(A + B \to \gamma + c + X) = \int dv dx_1 dx_2 \Bigg[ & \frac{d\Delta\sigma_{coll}^{cg\to\gamma c}}{dv} \\ & + \Delta f_g^A(x_1, M^2) \Delta f_c^B(x_2, M^2) \frac{d\Delta\sigma^{HO}}{dv}(cg \to \gamma c) \Bigg], \end{aligned} \tag{A4}$$

plus terms in which the beam and target are interchanged. We use subscript $c$ to label the charm (or anti-charm) quark.

We define

$$\Delta T_{cg} = \frac{v(2-v)}{1-v}, \tag{A5}$$

and $v_1 = 1 - v$. In Eq. (A4),

$$\begin{aligned}
\frac{d\Delta\sigma^{HO}}{dv}(cg \to \gamma c) = \frac{\pi\alpha_{em}\alpha_s e_c^2}{\hat{s}N_C}\Bigg(\Delta T_{cg} + \frac{\alpha_s}{2\pi}\Bigg[\frac{1}{2}\Big(&-14C_F\Delta T_{cg} + 2(2C_F + N_c)\ln^2\delta_s\Delta T_{cg} \\
&- \frac{2}{3}N_F\ln\frac{\hat{s}}{M^2}\Delta T_{cg} + C_F(3 + 4\ln\delta_s)\left(\ln\frac{\hat{s}}{M^2} + \ln\frac{\hat{s}}{M''^2}\right)\Delta T_{cg} \\
&+ \frac{N_c}{3}(11 + 12\ln\delta_s)\ln\frac{\hat{s}}{M^2}\Delta T_{cg} + \frac{1}{3}(11N_c - 2N_F)\ln\frac{\hat{s}}{\mu^2}\Delta T_{cg} \\
&+ (2C_F - N_c)\ln^2 v\Delta T_{cg} + 4\ln\delta_s(N_c\ln v_1 + 2C_F\ln v - N_c\ln v)\Delta T_{cg} \\
&+ 2(2C_F - N_c)\ln v_1\ln v\Delta T_{cg} - 2C_F\pi^2\frac{(3 - 4v - v^2)}{3v_1} \\
&+ N_c\pi^2\frac{(3 - 2v - 2v^2)}{3v_1} + \ln^2 v_1\left(N_c(1+v) - 2C_F\frac{(1-2v)}{v_1}\right) \\
&+ \ln v_1\left(2N_c + 2C_F\frac{(1+2v)}{v_1}\right) + 2(2C_F - N_c)\Delta T_{cg}\mathrm{Li}_2(v_1) \\
&+ 2N_c\Delta T_{cg}\mathrm{Li}_2(v)\Big)\Bigg]\Bigg).
\end{aligned} \tag{A6}$$

The scales $M$ and $M''$ are the factorization and fragmentation scales, respectively, on the initial parton and final-state charm quark legs, and $\mu$ is the renormalization scale. $C_F = 4/3$ is the quark-gluon vertex color factor, $N_C = 3$ is the number of colors, $e_c$ is the fractional charge of the charm quark, $\delta_s$ and $\delta_c$ are the soft and collinear cutoff parameters introduced in Sec. II, $\mathrm{Li}_2(x)$ is the dilogarithm function, and $\alpha_{em}$ is the electromagnetic coupling constant.

The remnants of the factorization of the hard collinear singularities are

$$\begin{aligned}
\frac{d\Delta\sigma_{coll}^{cg\to\gamma c}}{dv} = \frac{\alpha_{em}\alpha_s^2 e_c^2}{2\hat{s}}\frac{1}{N_C}\Delta T_{cg}\Bigg[&\Delta f_g^A(x_1, M^2)\left(\int_{x_2}^{1-\delta_s}\frac{dz}{z}\Delta f_c^B\left(\frac{x_2}{z}, M^2\right)\Delta\tilde{P}_{qq}(z)\right. \\
&\left. + \int_{x_2}^{1}\frac{dz}{z}\Delta f_g^B\left(\frac{x_2}{z}, M^2\right)\Delta\tilde{P}_{qg}(z)\right) \\
&+ \Delta f_c^B(x_2, M^2)\left(\int_{x_1}^{1-\delta_s}\frac{dz}{z}\Delta f_g^A\left(\frac{x_1}{z}, M^2\right)\Delta\tilde{P}_{gg}(z)\right. \\
&\left. + \int_{x_1}^{1}\frac{dz}{z}\Delta f_q^A\left(\frac{x_1}{z}, M^2\right)\Delta\tilde{P}_{gq}(z)\right)\Bigg].
\end{aligned} \tag{A7}$$

The last distribution,$\Delta f_q^A(x_1, M^2)$, in Eq. (A7) implies a sum over the flavors of quarks from

the $cc$, $cq$, and $c\bar{q}$ initial states. The remaining two processes, $c\bar{c}$ and $q\bar{q}$, do not have initial state collinear singularities and thus do not contribute to this part of the cross section.

The polarized splitting functions $\Delta\tilde{P}_{ij}$, are

$$\Delta\tilde{P}_{ij}(z) = \Delta P_{ij}(z) \ln\left(\frac{1-z}{z}\delta_c\frac{\hat{s}}{M^2}\right) - \Delta P'_{ij}(z). \tag{A8}$$

The functions $\Delta P_{ij}(z,\epsilon)$, the spin dependent Altarelli-Parisi splitting functions in $4-2\epsilon$ dimensions, are

$$\begin{aligned}
\Delta P_{qq}(z,\epsilon) &= C_F\left[\frac{1+z^2}{1-z} + 3\epsilon(1-z)\right] \\
\Delta P_{qg}(z,\epsilon) &= \frac{1}{2}\left[(2z-1) - 2\epsilon(1-z)\right] \\
\Delta P_{gg}(z,\epsilon) &= 2N_C\left[\frac{1}{1-z} - 2z + 1 + 2\epsilon(1-z)\right] \\
\Delta P_{gq}(z,\epsilon) &= C_F\left[(2-z) + 2\epsilon(1-z)\right].
\end{aligned} \tag{A9}$$

The functions $\Delta P'_{ij}(z)$ are defined by the relation

$$\Delta P_{ij}(z,\epsilon) = \Delta P_{ij}(z) + \epsilon\Delta P'_{ij}(z). \tag{A10}$$

### 2. Pseudo-Two-Body Contributions

Since we are interested in distributions in the kinematic variables of two final-state partons, the photon and the $c$ quark, we can define variables that depend on the momenta of both. An example is the variable $z$, defined by

$$z = -\frac{p_T^\gamma . p_T^c}{|p_T^\gamma|^2}. \tag{A11}$$

Whenever there is a third parton in the final state, the distribution in $z$ (or in other analogous variables) will differ from a $\delta$ function when the third parton carries a finite momentum, even if it is collinear to one of the other final partons. For this reason we designate as "pseudo-two-body contributions" those for which the third parton is collinear to either the final photon or the charm quark. These contributions are expressed, respectively, by the equations

$$\Delta\sigma_{\gamma/coll} = \sum_{abcq} \int \Delta f_a^A(x_1, M^2) \Delta f_b^B(x_2, M^2) \left(\frac{\alpha_{em}}{2\pi}\right) \left[P_{\gamma q}(z) \ln\left[z(1-z)\delta_c \frac{\hat{s}}{M'^2}\right] - P'_{\gamma/q}(z)\right] \times \frac{d\hat{\Delta\sigma}}{dv}(ab \to cq) dx_1 dx_2 dz dv, \tag{A12}$$

and

$$\Delta\sigma_{c/coll} = \sum_{abd} \int \Delta f_a^A(x_1, M^2) \Delta f_b^B(x_2, M^2) \tilde{P}_{cd}(z, M''^2) \frac{d\Delta\hat{\sigma}}{dv}(ab \to \gamma d) dx_1 dx_2 dz dv. \tag{A13}$$

The functions $P_{\gamma/q}(z)$ and $P'_{\gamma/q}(z)$ are the quark-to-photon splitting function and $O(\epsilon)$ piece, respectively. They have the same form as $P_{gq}$, with the color factor replaced by the square of the quark charge. The scale $M'$ is the fragmentation scale for quark fragmentation into a photon. In Eq. (A13),

$$\tilde{P}_{cd}(z, M''^2) = P_{cd}(z) \ln\left[z(1-z)\delta_c \frac{s}{M''^2}\right] - P'_{cd}(z), \tag{A14}$$

where $P_{cd}(z)$ represents the splitting functions $P_{qg}(z)$ and $P_{qq}(z)$. The unpolarized splitting functions are

$$\begin{aligned} P_{qq}(z,\epsilon) &= C_F \left[\frac{1+z^2}{1-z} - \epsilon(1-z)\right] \\ P_{qg}(z,\epsilon) &= \frac{1}{2(1-\epsilon)} \left[z^2 + (1-z)^2 - \epsilon\right] \\ P_{gg}(z,\epsilon) &= 2N_C \left[\frac{z}{1-z} + \frac{1-z}{z} + z(1-z)\right] \\ P_{gq}(z,\epsilon) &= C_F \left[\frac{1+(1-z)^2}{z} - \epsilon z\right]. \end{aligned} \tag{A15}$$

The functions $P'_{ij}(z)$ are defined by the relation

$$P_{ij}(z,\epsilon) = P_{ij}(z) + \epsilon P'_{ij}(z). \tag{A16}$$

In Eq. (A12), $q$ can be a charm quark or a charm anti-quark, or a(an) (anti)quark of any flavor in the case of $cq \to cq$. In Eq. (A13), $d$ is either a gluon, a charm quark, or a charm antiquark. Note that the splitting functions $P_{\gamma/q}$ and $P_{cd}$ are the usual spin averaged and not the spin dependent ones, since the final state is not polarized.

These contributions are referred to usually as the remnants of the factorization of the hard collinear singularities and are regarded as two-body processes, or as parts of the fragmentation contributions because of their dependence on the factorization scales. We prefer to regard them as pseudo-two-body contributions. When we examine either the charm quark or photon momentum distributions, these contributions populate the same regions of phase space as the other three-body contributions in Eq. (A20), unlike the effective two-body contributions. The pseudo-two-body contributions are usually negative in overall sign due to the large logarithms of the cut-off parameters, as are the two-body contributions discussed above.

### 3. Photon Fragmentation Contributions

As mentioned in Sec. II, we include the quark-to-photon and gluon-to-photon fragmentation contributions at leading order only. We convolute the $2 \to 2$ hard scattering subprocess cross sections for the processes listed in Eq. (2.7) with photon fragmentation functions $D_{\gamma/i}(z, M'^2)$; $M'$ is the fragmentation scale, the same scale at which we subtract the collinear singularities on the photon leg of the three-body processes. The expression for the cross section is

$$\Delta\sigma_{frag/\gamma} = \sum_{abj} \int \Delta f_a^A(x_1, M^2) \Delta f_b^B(x_2, M^2) D_{\gamma/j}(z, M'^2) \frac{d\Delta\hat{\sigma}}{dv}(ab \to jc) dx_1 dx_2 dz dv. \quad \text{(A17)}$$

The matrix elements for the hard subprocess cross section can be found, for example, in Ref. [20].

### 4. Charm Fragmentation Contributions

In integrating some of the three-body matrix elements over phase space we encounter configurations in which the produced charm quark is collinear with an anti-charm quark or a gluon in the final state. These situations lead to a collinear singularity in the massless approximation. They occur for the processes of Eq. (2.1a), (2.1c), and (2.1f). We factor

these singularities into a fragmentation function $D_{c/i}(z, M''^2)$ for parton $i$ to produce a charm quark with momentum fraction $z$. The contributing subprocess cross sections are

$$\frac{d\Delta\hat{\sigma}}{dv}(q\bar{q} \to \gamma g) = -\frac{2C_F}{N_C}\frac{\pi\alpha\alpha_s e_q^2}{s}\left(\frac{v}{1-v} + \frac{1-v}{v}\right);$$
$$\frac{d\Delta\hat{\sigma}}{dv}(qg \to \gamma q) = \frac{\pi\alpha\alpha_s e_q^2}{N_C s}\left(\frac{1-(1-v)^2}{1-v}\right). \tag{A18}$$

The physical cross section is given by

$$\Delta\sigma_{frag/c} = \sum_{abd}\int \Delta f_a^A(x_1, M^2)\Delta f_b^B(x_2, M^2)D_{c/d}(z, M''^2)\frac{d\Delta\hat{\sigma}}{dv}(ab \to \gamma d)dx_1dx_2dzdv. \tag{A19}$$

### 5. Three-body contributions

The non-collinear three-body final-state contributions are calculated from the expression

$$\Delta\sigma_{3body} = \sum_{abd}\int \Delta f_a^A(x_1, M^2)\Delta f_b^B(x_2, M^2)d\Delta\hat{\sigma}(ab \to \gamma cd)dx_1dx_2d\Omega, \tag{A20}$$

with $\Omega$ representing the angles and other variables that are integrated over. Whenever an invariant $s_{ij}$ or $t_{ij}$ falls into a collinear or soft region of phase space, that contribution from the subprocess is excluded. The three-body contribution shows no dependence on the factorization scale of the final-state charm or photon legs, although we have factored collinear singularities at scales $M''$ and $M'$, respectively, on these legs of the three-body subprocesses. However, Eq. (A20) does contain implicit logarithmic dependence on the soft and, in particular, the collinear cutoffs discussed in Sec. II. Both collinear cutoff and factorization scale dependences are contained in the pseudo-two-body contributions discussed above.

# REFERENCES


[1] E. L. Berger and J.-W. Qiu, Phys. Lett. **B248**, 371 (1990) and Phys. Rev. **D44**, 2002 (1991); H. Baer, J. Ohnemus, and J. F. Owens, Phys. Rev. **D42**, 61 (1990); P. Aurenche *et al*, Nucl. Phys. **B399**, 34 (1993); L. E. Gordon and W. Vogelsang, Phys. Rev. **D48**, 3136 (1993) and **D50**, 1901 (1994); M. Glück, L. E. Gordon, E. Reya, and W. Vogelsang, Phys. Rev. Lett. **73**, 388 (1994); L. E. Gordon, Nucl. Phys. **B501**, 175 (1997).

[2] E. L. Berger and J.-W. Qiu, Phys. Rev. **D40**, 778 (1989).

[3] L. E Gordon and W. Vogelsang, Phys. Lett. **B387**, 629 (1996).

[4] E. L. Berger and L. E. Gordon, Phys. Rev. **D54**, 2279 (1996).

[5] B. Bailey, E. L. Berger, and L. E. Gordon, Phys. Rev. **D54**, 1896 (1996) and references therein.

[6] E. L. Berger, E. Braaten, and R. D. Field, Nucl. Phys. **B239**, 52 (1984).

[7] D.W. Duke and J. F. Owens, Phys. Rev. **D26**, 1600 (1982); J. F. Owens, Rev. Mod. Phys. **59**, 465 (1987).

[8] P. Aurenche *et al*, Nucl. Phys. **B399**, 34 (1993).

[9] M. Glück, E. Reya, and A. Vogt, Phys. Rev. **D48**, 116 (1993).

[10] E. L. Berger and J.-W. Qiu, Phys. Lett. **B248**, 371 (1990) and Phys. Rev. **D44**, 2002 (1991); E. L. Berger, X. Guo, and J.-W. Qiu, Phys. Rev. Lett. **76**, 2234 (1996).

[11] H. Baer, J. Ohnemus, and J. F. Owens, Phys. Rev. **D42**, 61 (1990).

[12] L. E. Gordon, Nucl. Phys. **B501**, 175 (1997).

[13] H. Baer, J. Ohnemus, and J. F. Owens, Phys. Lett. **B234**, 127 (1990).

[14] L. E. Gordon, Phys. Lett. **B406**, 184 (1997); S. Chang, C. Coriano, and L. E. Gordon, Argonne report ANL-HEP-PR-97-21 (Phys. Rev. D, to be published).

[15] B. Bailey, J. Ohnemus, and J. F. Owens, Phys. Rev. **D46**, 2018 (1992).

[16] C. Coriano and L. E. Gordon, Nucl. Phys. **B469**, 202 (1996); Phys. Rev. **D54**, 781 (1996).

[17] H. Baer and H. Reno, Phys. Rev. **D43**, 2892 (1991).

[18] J. Ohnemus and J. F. Owens, Phys. Rev. **D43**, 3626 (1991); J. Ohnemus, Phys. Rev. **D44**, 1403 (1991); J. Ohnemus, Phys. Rev. **D44**, 3477 (1991).

[19] T. Gehrmann and W. J. Stirling, Phys. Rev. **D53**, 6100 (1996).

[20] L. E. Gordon and W. Vogelsang, Phys. Rev.**D50**, 1901 (1994); M. Glück, L. E. Gordon, E. Reya, and W. Vogelsang, Phys. Rev. Lett. **73**, 388 (1994).

[21] L. E. Gordon, Nucl. Phys. **B501**, 197 (1997).

[22] P. Aurenche, R. Baier, A. Douiri, M. Fontannaz, and D. Schiff, Phys. Lett. **B140**, 87 (1984); P. Aurenche, R. Baier, M. Fontannaz, and D. Schiff, Nucl. Phys. **B297**, 661 (1988).

[23] L. E. Gordon and W. Vogelsang, Phys. Rev. **D48**, 3136 (1993) and **D49**, 170 (1994).

[24] G. 'tHooft and M. Veltman, Nucl. Phys. **B44**, 189 (1972).

[25] P. Breitenlohner and D. Maison, Commun. Math Phys. **52**, 11 (1977).

[26] L. E. Gordon, work in progress.

[27] A. P. Contogouris, B. Kamal, Z. Merebashvili, and F. V. Tkachov, Phys. Lett. **B304**, 329 (1993); Phys. Rev. **D48**, 4092 (1993).

[28] G. Altarelli and G. Parisi, Nucl. Phys. **B126**, 298 (1977).

[29] E. L. Berger, Phys. Rev. **D37**, 1810 (1988).

[30] A parametrization, not yet available for general use, that includes a charm component

is reported in L. E. Gordon, M. Goshtasbpour, and G. P. Ramsey, Argonne report ANL-HEP-PR-98-08.

[31] H. L. Lai *et al*, Phys. Rev. **D55**, 1280 (1997).

[32] L. E. Gordon and G. P. Ramsey, work in progress.

# FIGURE CAPTIONS

[1] (a) Lowest order Feynman diagrams for $\gamma$ plus $c$ quark production; $k_1$ and $k_2$ are the four-vector momenta of the photon and charm quark. (b) Examples of virtual corrections to the lowest order diagrams. (c) Examples of next-to-leading order three-body final-state diagrams for the $gc$ initial state.

[2] (a) Ratio of the polarized to the unpolarized gluon distribution $\Delta G(x,\mu)/G(x,\mu)$ at $\mu^2 = 100$ GeV$^2$ for the GSA, GSB and GSC spin-dependent parton distributions and the CTEQ4M spin-averaged distributions. Evolution begins at $\mu_o = 1.5$ GeV, and the number of flavors $n_f$ is set to 4 in the evolution. (b) Same as (a) but for the charm distributions. The charm quark density is generated from bremsstrahlung of gluons into charm-anticharm pairs.

[3] (a) Spin-averaged cross section $d\sigma/dp_T^\gamma$ as a function of the transverse momentum of the photon for $p + p \rightarrow \gamma + c + X$ at $\sqrt{S} = 200$ GeV. The transverse momentum of the charm quark is restricted to $p_T^c > 5$ GeV, and the rapidities of the photon and charm quark are restricted to the interval $-1.0 < y < 1.0$. Two curves are drawn. The solid curve shows the cross section that results from the inclusion of all subprocesses through $O(\alpha_s^2)$, and the dashed curve shows the contribution from the dominant $cg$ subprocess, only, through $O(\alpha_s^2)$. (b) For the same selections as in (a), the two-spin longitudinal asymmetry is shown for the three choices of the spin-dependent gluon density. In the case of GSA, the dot-dashed curve shows the contribution to $A_{LL}$ from the $cg$ subprocess only. (c) For the same selections as in (a), the two-spin longitudinal asymmetry $A_{LL}$ is shown for the GSC spin-dependent gluon density (dotted line), along with the contribution from the $cg$ subprocess only.

[4] (a) Spin-averaged cross section $d\sigma/dy^c$ as a function of the rapidity of the charm quark for $p+p \rightarrow \gamma+c+X$ at $\sqrt{S} = 200$ GeV. The photon rapidity is restricted

to $-1.0 < y^\gamma < 1.0$, and $4 < p_T^\gamma < 50$ GeV. The transverse momentum of the charm quark is selected to be in the region $p_T^c > 5$ GeV. The solid curve shows the cross section that results from the inclusion of all subprocesses through $O(\alpha_s^2)$, and the dashed curve shows the contribution from the dominant $cg$ subprocess through $O(\alpha_s^2)$. (b) For the same selections as in (a), the two-spin longitudinal asymmetry is shown for the three choices of the spin-dependent gluon density. The solid, dashed, and dotted curves represent the results from calculations based on our modified GSA, GSB, and GSC densities, respectively. In the GSA case, the dot-dashed curve shows the contribution to $A_{LL}$ from the $cg$ subprocess only.

[5] (a) Spin-averaged cross section $d\sigma/d\Delta y$ as a function of the difference $\Delta y = y^c - y^\gamma$ of the rapidities of the photon and charm quark, for $p + p \to \gamma + c + X$ at $\sqrt{S} = 200$ GeV. The transverse momentum of the photon is selected to be in the interval, $4 < p_T^\gamma < 50$ GeV, and its rapidity is restricted to $-1.0 < y^\gamma < 1.0$. The transverse momentum of the charm quark satisfies $p_T^c > 5$ GeV. The solid curve shows the cross section that results from the inclusion of all subprocesses, and the dashed curve shows the contribution from the dominant $cg$ subprocess only. (b) For the same selections as in (a), the two-spin longitudinal asymmetry is shown for the three choices of the spin-dependent gluon density. The solid, dashed, and dotted curves represent the results from calculations based on our modified GSA, GSB, and GSC densities, respectively.

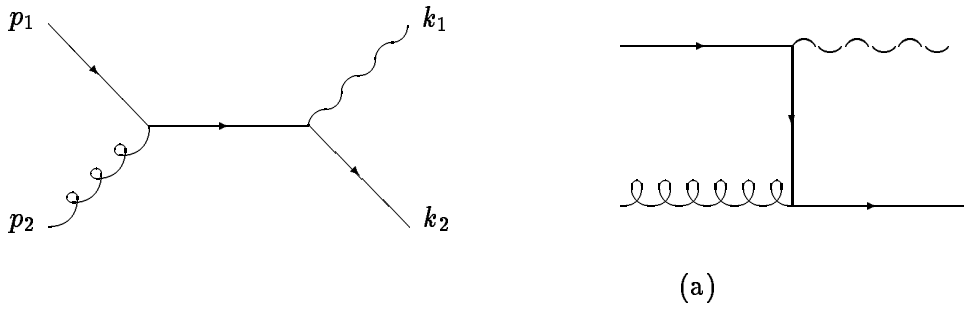


(a)

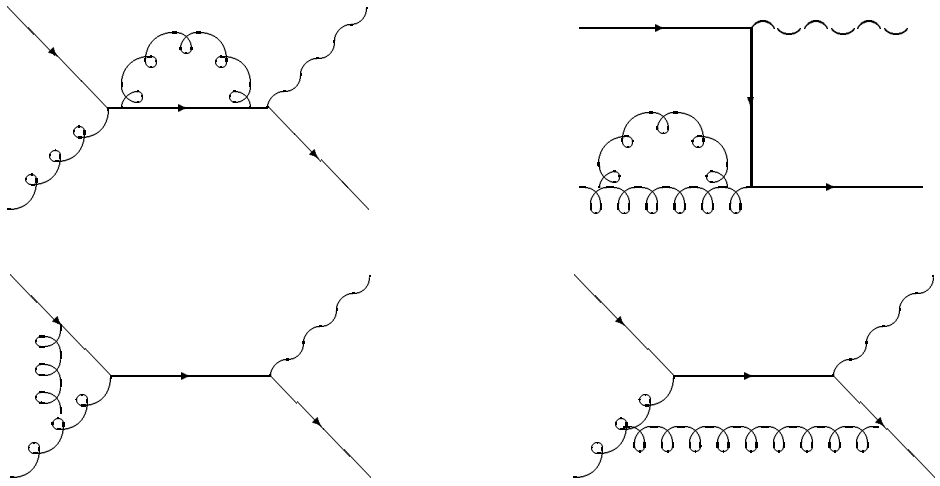

(b)

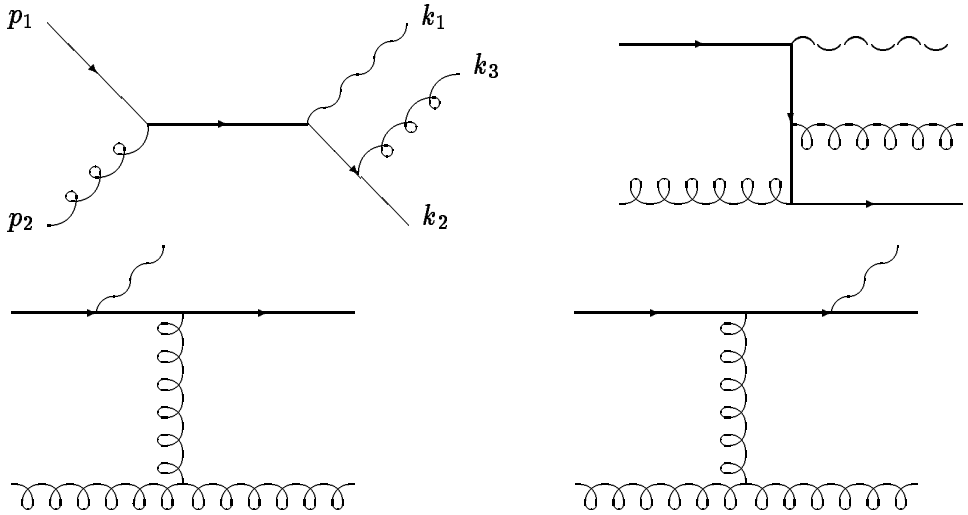


(c)

Fig.1

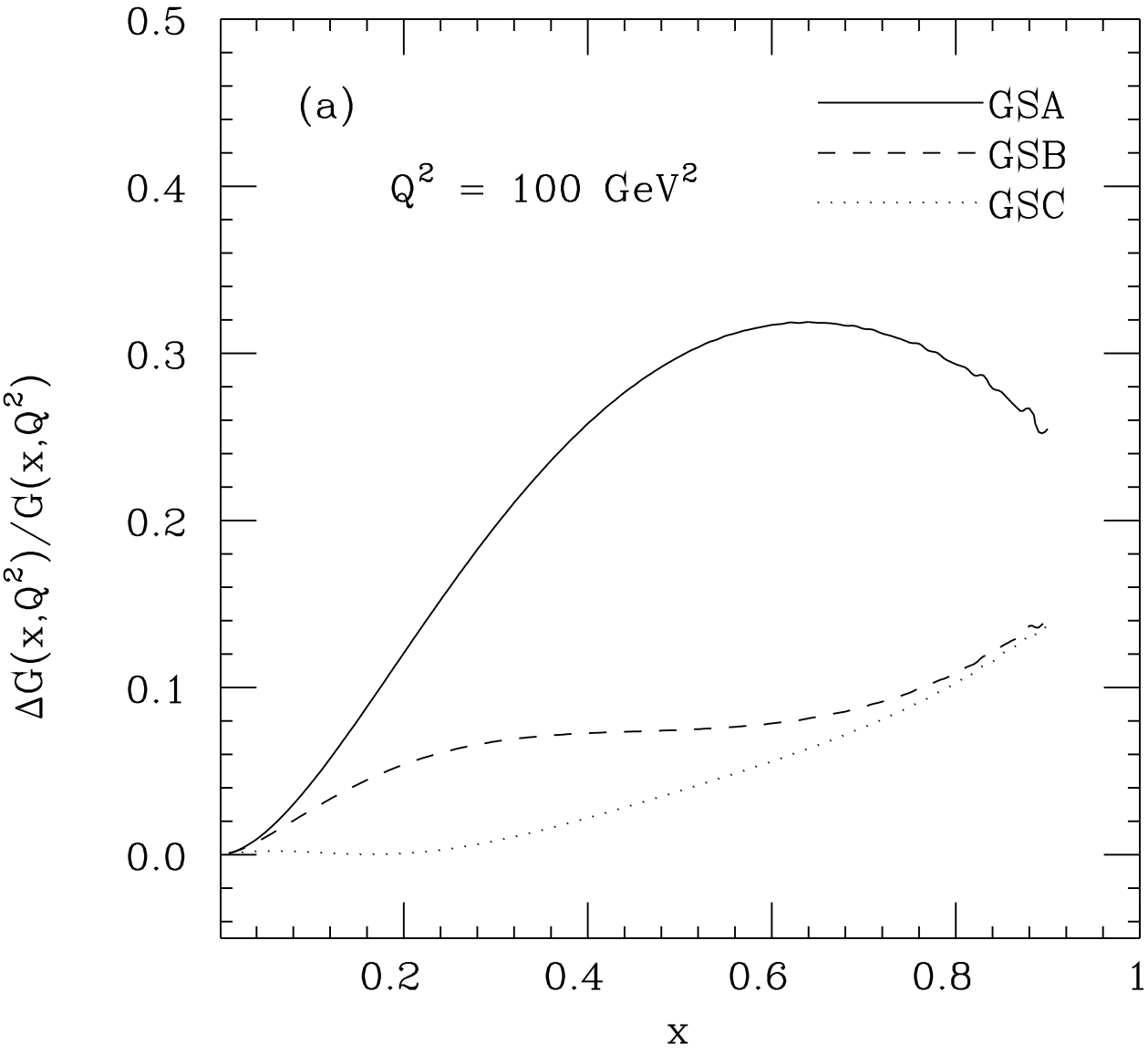
(a)
$Q^2$ = 100 GeV$^2$
GSA
GSB
GSC
$\Delta G(x,Q^2)/G(x,Q^2)$
x
0.0
0.1
0.2
0.3
0.4
0.5
0.2
0.4
0.6
0.8
1

Fig. 2a

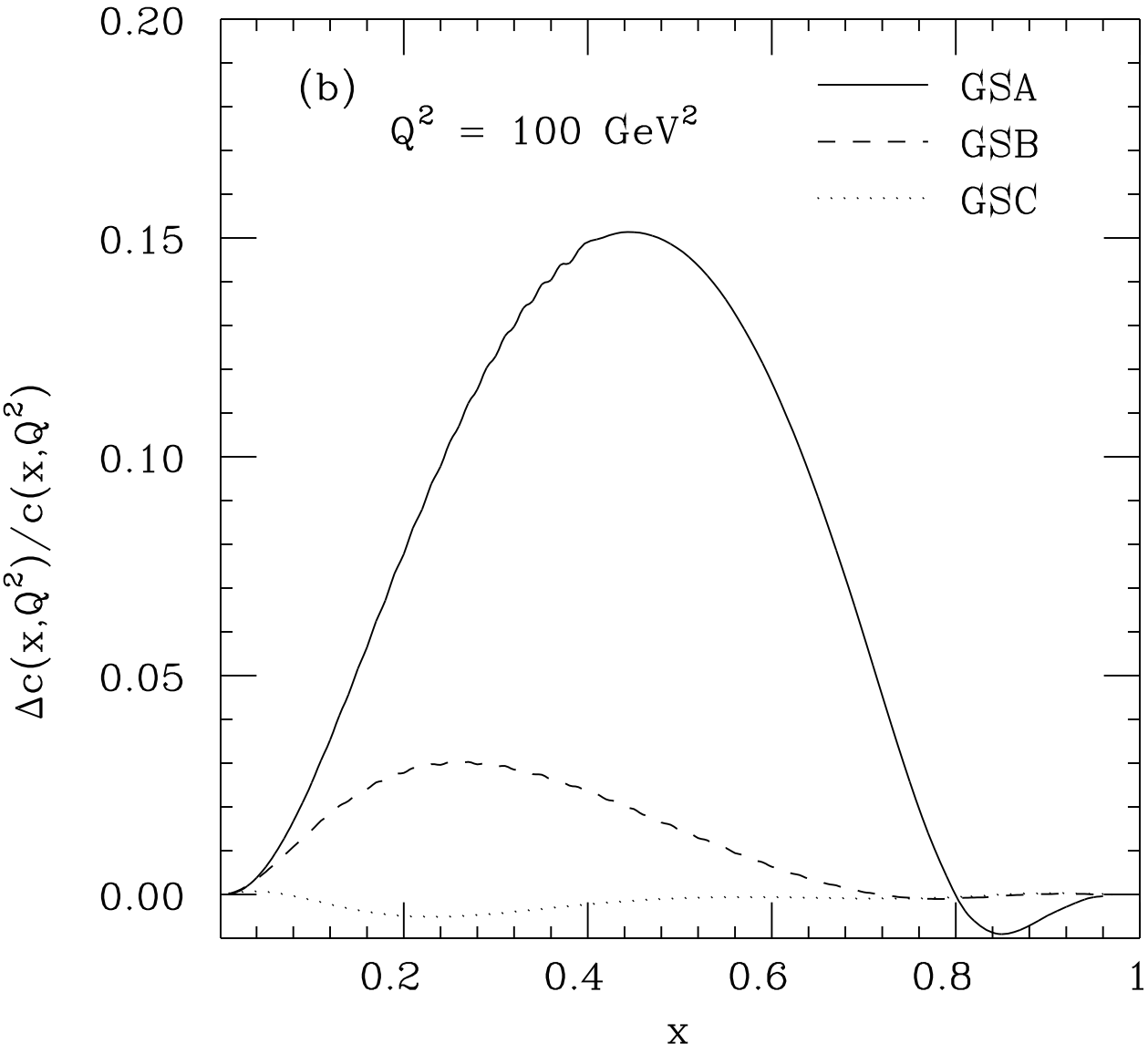
(b)
$Q^2$ = 100 GeV$^2$
GSA
GSB
GSC
0.20
0.15
0.10
0.05
0.00
0.2
0.4
0.6
0.8
1
x
$\Delta c(x,Q^2)/c(x,Q^2)$

Fig. 2b

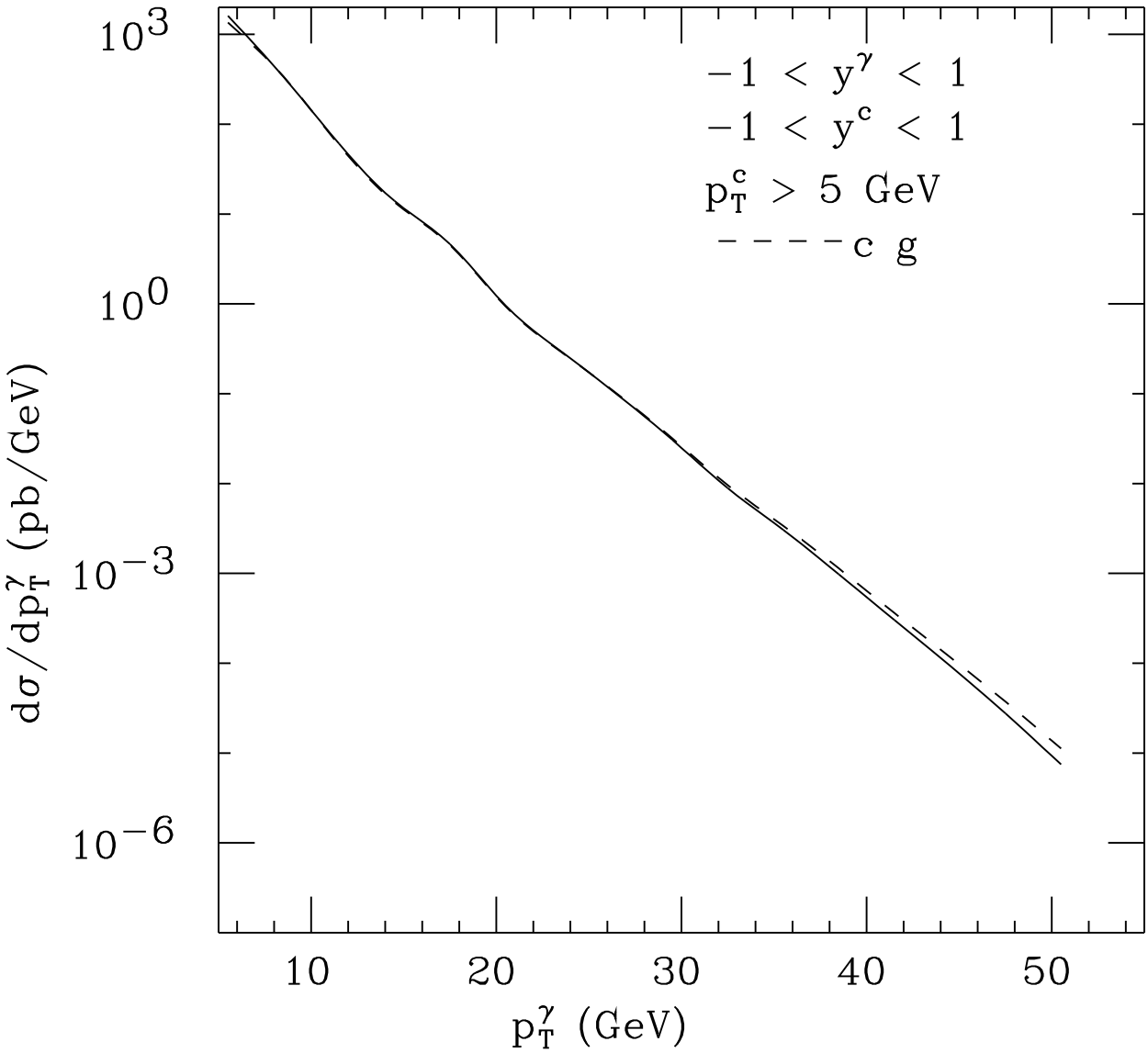
$10^3$
$10^0$
$10^{-3}$
$10^{-6}$
$d\sigma/dp_T^\gamma$ (pb/GeV)
$-1 < y^\gamma < 1$
$-1 < y^c < 1$
$p_T^c > 5$ GeV
c g
10
20
30
40
50
$p_T^\gamma$ (GeV)

Fig. 3a

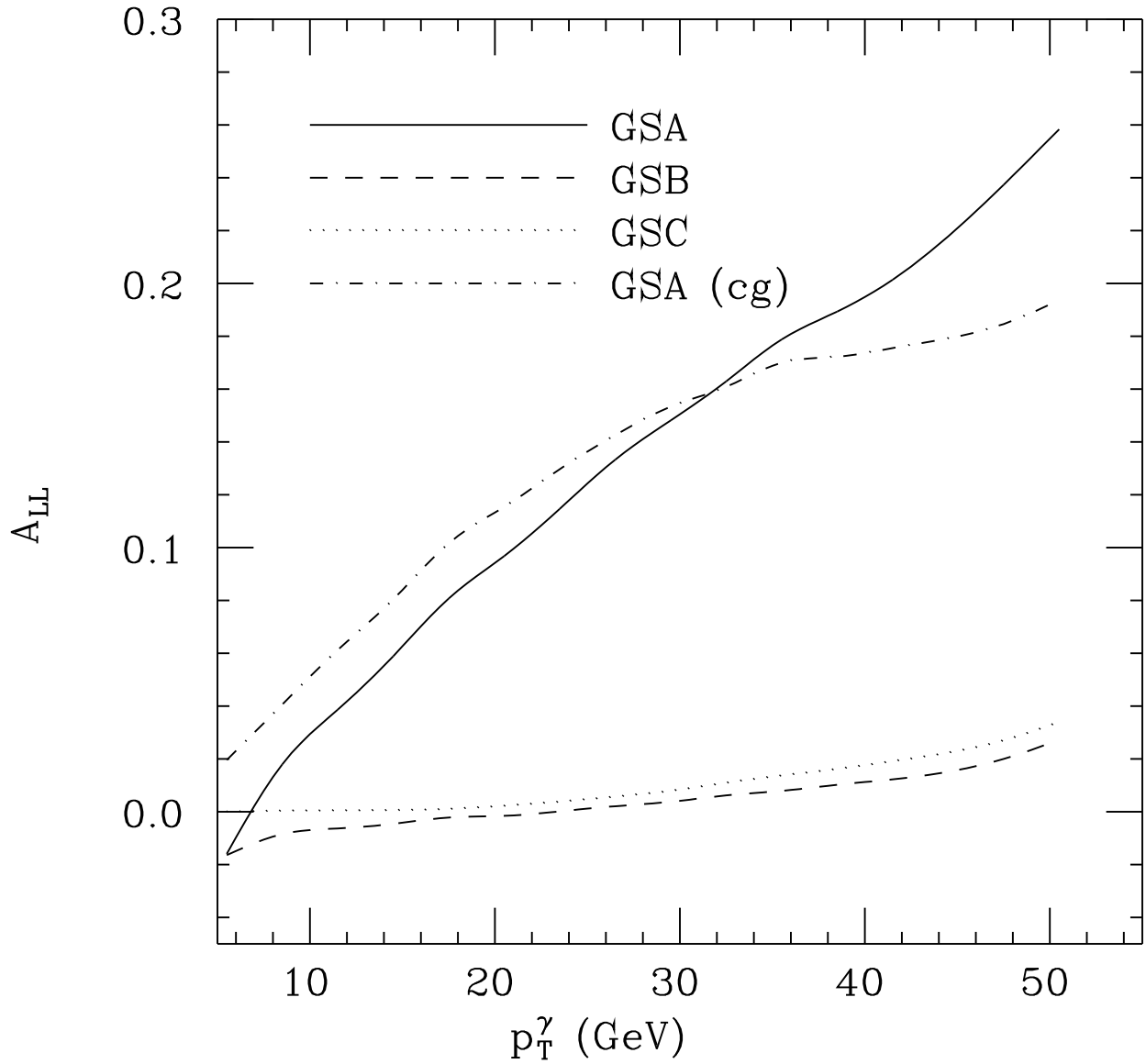


Fig. 3b

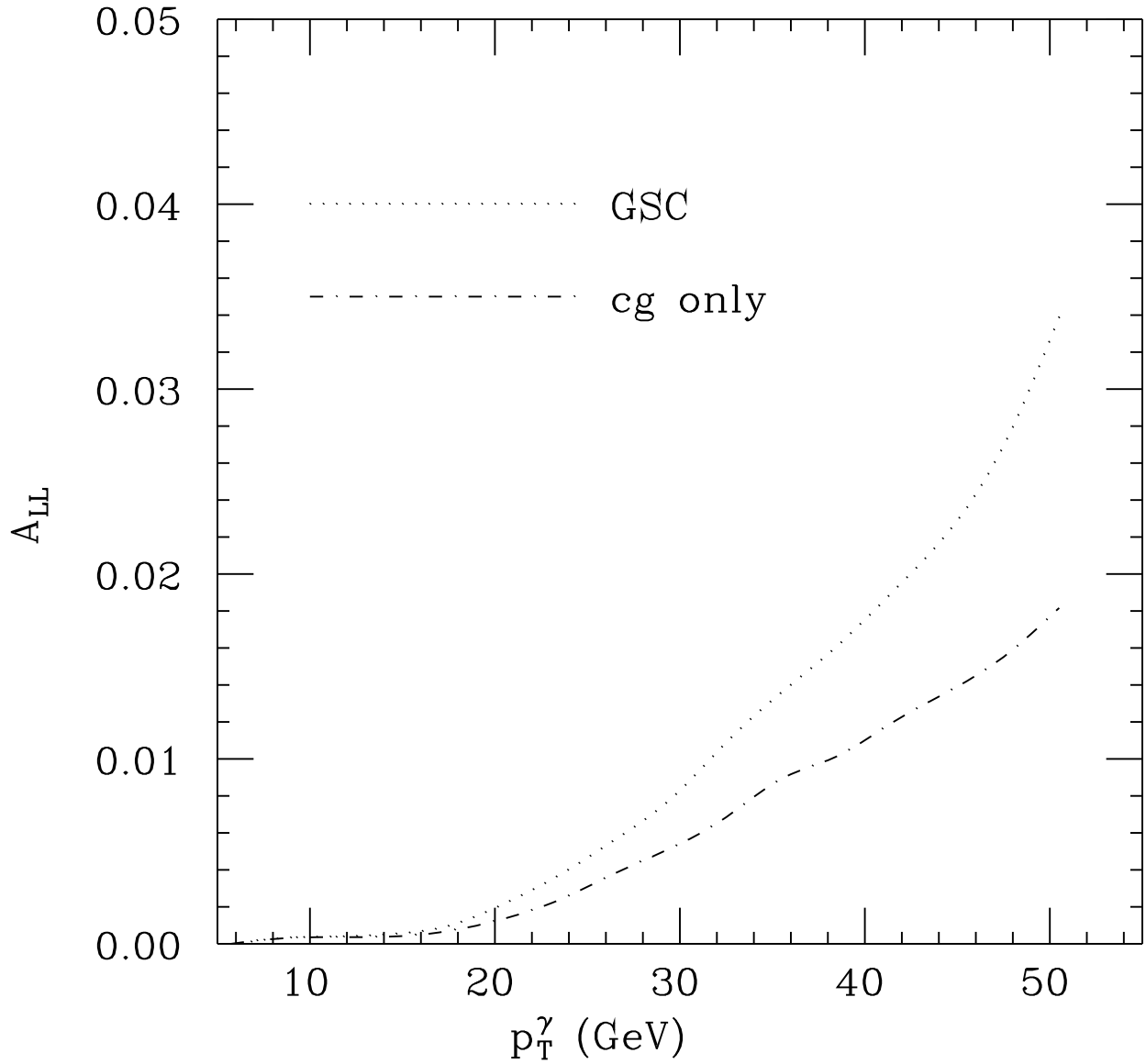
0.05
0.04
0.03
0.02
0.01
0.00
$A_{LL}$
GSC
cg only
10
20
30
40
50
$p_T^\gamma$ (GeV)

Fig. 3c

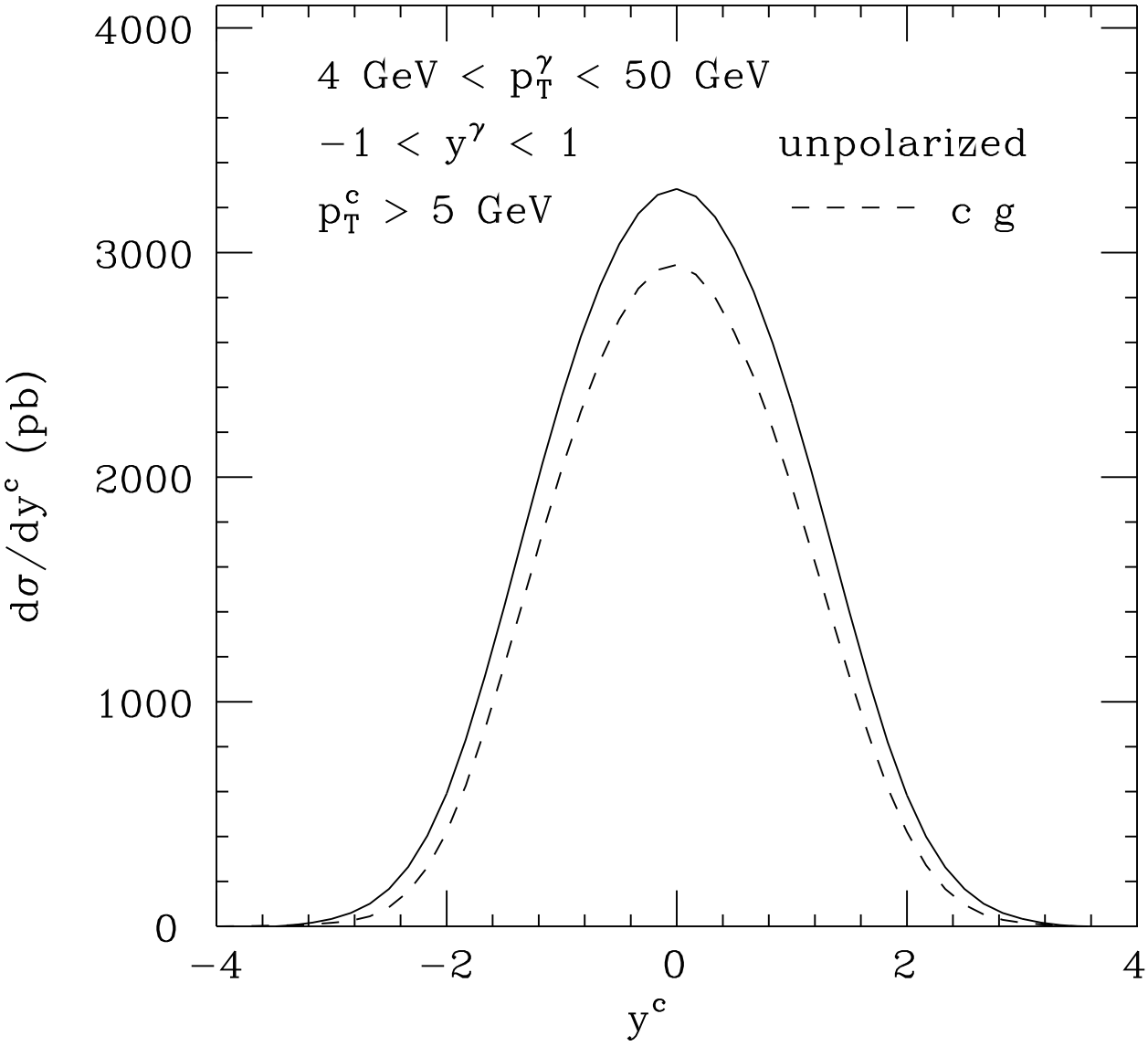
4000
3000
2000
1000
0
−4
−2
0
2
4
4 GeV < $p_T^\gamma$ < 50 GeV
−1 < $y^\gamma$ < 1
$p_T^c$ > 5 GeV
unpolarized
c g
$d\sigma/dy^c$ (pb)
$y^c$

Fig. 4a

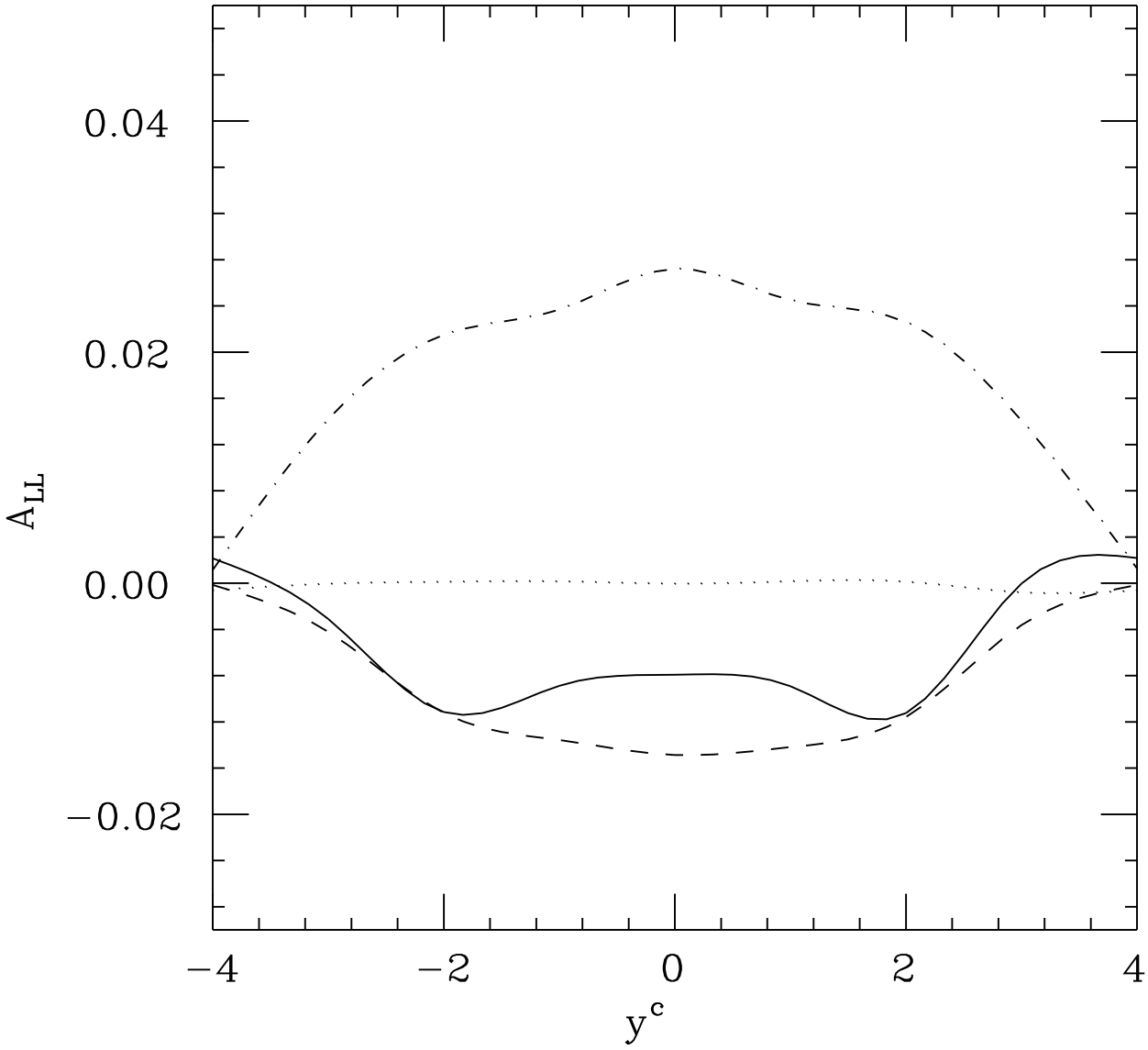


Fig. 4b

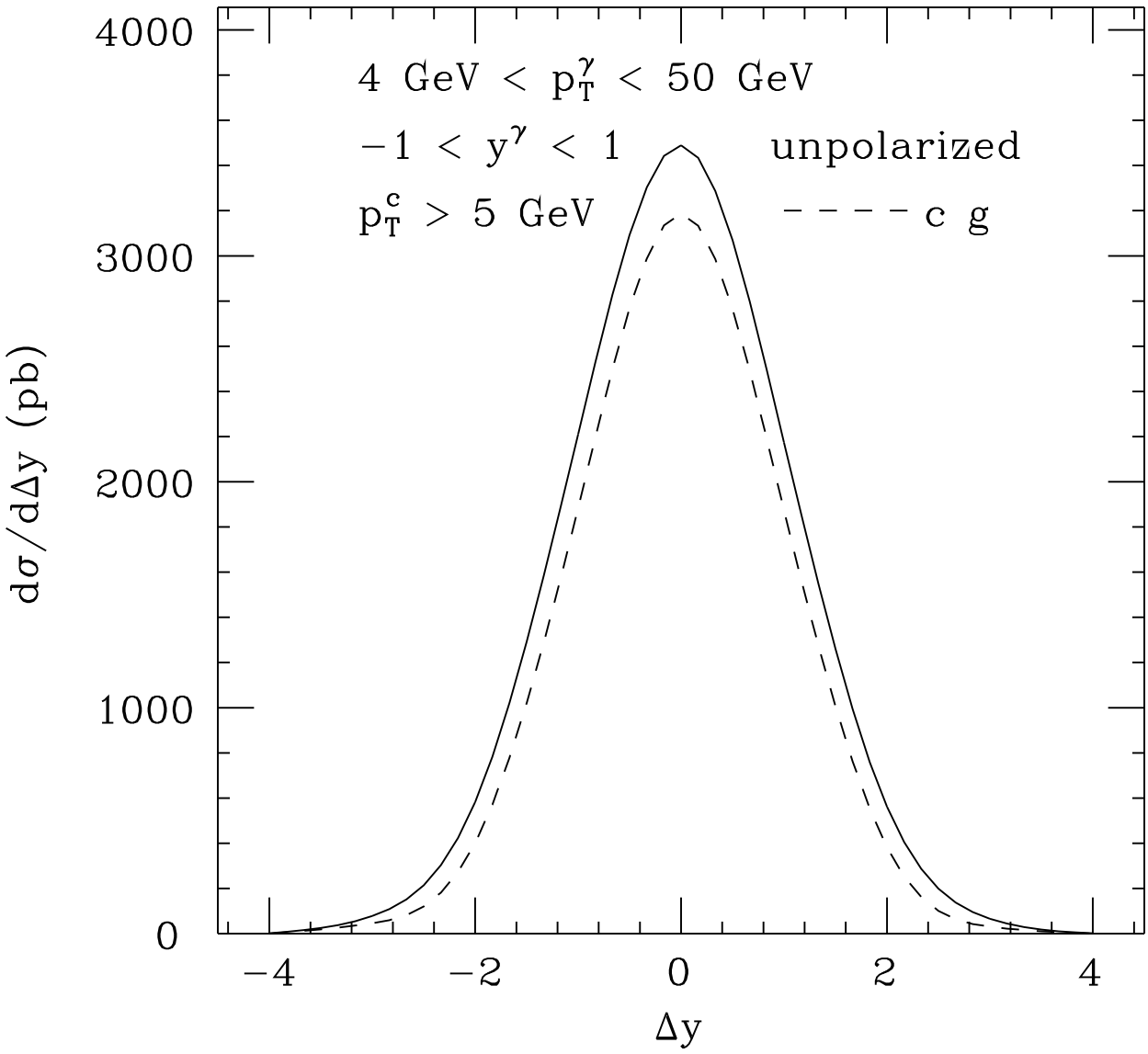
4000
3000
2000
1000
0
−4
−2
0
2
4
Δy
dσ/dΔy (pb)
4 GeV < $p_T^\gamma$ < 50 GeV
−1 < $y^\gamma$ < 1
$p_T^c$ > 5 GeV
unpolarized
c g

Fig. 5a

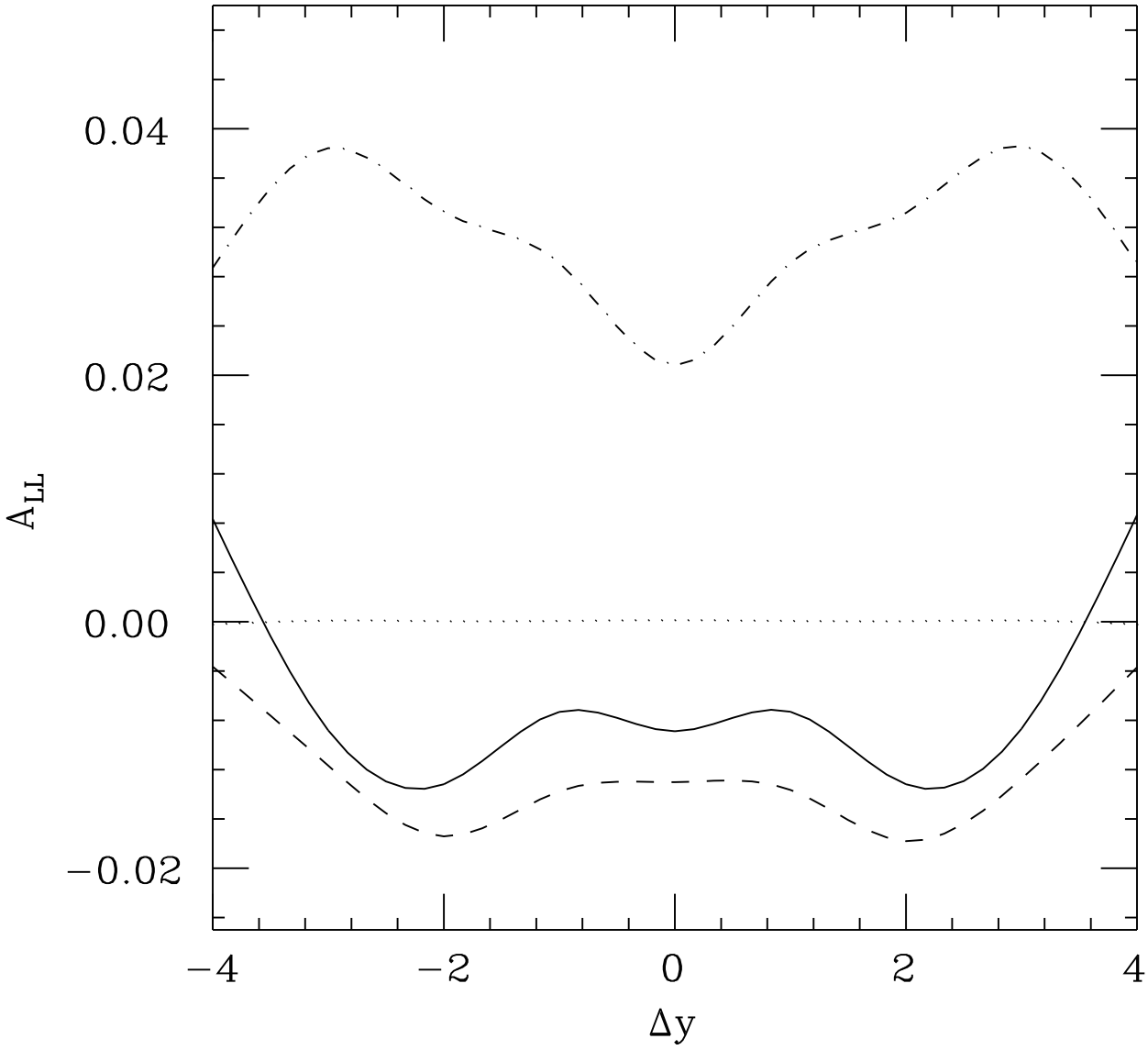


Fig. 5b